Control of Inertial Stabilization Systems Using Robust Inverse Dynamics Control and Adaptive Control

Prasatporn Wongkamchang and Viboon Sangveraphunsiri
Department of Mechanical Engineering, Chulalongkorn University,
Bangkok 10330, Thailand.
Email: viboon.s@eng.chula.ac.th

Abstract

This paper presents an advanced controller design for an Inertial stabilization system. The system has a 2-DOF gimbal which will be attached to an aviation vehicle. Due to dynamics modeling errors, and friction and disturbances from the outside environment, the tracking accuracy of an airborne gimbal may severely degrade. So, an advanced controller is needed. A robust inverse dynamics control and the adaptive control are used in the inner loop or gimbal servo-system to control the gimbal motion. An indirect line of sight (LOS) stabilization will be controlled by the outer loop controller. A stabilizer is mounted on the base of the system to measure base rate and orientation of the gimbal in reference to the fixed reference frame. It can withstand high angular slew rates. The experimental results illustrate that the proposed controllers are capable enough to overcome the disturbances and the impact of LOS disturbances on the tracking performance.

Keywords: Inertial Stabilization, Gimbal

1. Introduction

Surveying of forest resources, and flood or other surveys by air must have either a forester and a wild expert or a camera and other useful instruments to go upon the aircraft in order to record pictures for analyzing. Doing these things are wasting a lot of both time and budget. Moreover, they may lead to the loss of valuable personnel and assets if the aircraft faces harmful situations. At the present, a camera gimbal is set up into the aircraft structure. Additionally, the motion of the camera can be controlled remotely from a ground station as well as the airplane. The camera gimbal can also send tremulous pictures to the ground by using a long-range data communication system. In this regard, it is very convenient for a variety of survey applications. The camera gimbal consists of two important parts. The first one is the gimbal mechanism with camera and sensor installed at the center of the gimbal mechanism. Another one is the image programming which stabilizes images. Since a moving platform will induce acceleration, friction forces and forces due to mass imbalance, these effects will be classified as disturbances to the input and need to be suppressed.

Motion control can be divided into 2 parts. The first part is controlled by a feedback control system in order to move the gimbal according to a reference command and in the same time to stabilize the gimbal where the camera is attached. Jittter reduction also is needed to be considered in this controller. The second part is the stabilizing of images done by an image programming technique, which will not be covered in this paper.

There are many works that have been done in this area, such as Do Li, David Hullender, Mike Direnzo [2] purposed a nonlinear induced disturbance rejection, H. Ambrose, Z. Qu, R. Johnson [5] purposed a nonlinear robust control, T.H. Lee, E.K. Koh, M.K. Loh. [6] purposed a stable adaptive control and Bo Li, David Hullender [8] purposed a self-turning controller for nonlinear inertial stabilization system. Jasim Ahmed, Dennis S. Bernstein worked on adaptive control for a system with unbalanced rotor.

This paper focuses on two controllers, the robust inverse dynamics control and the adaptive control, for stabilizing the servo loop. A stabilizer or rate sensor is mounted on the base of the system to measure the disturbance. The stabilizer can withstand high angular rates generated during slew and is equipped with a processor to transform the measurement to an equivalent disturbance about the LOS.

2. Two-Axis Camera Gimbal System

The camera gimbal consists of two joints: an outer joint attached to the azimuth axis and an inner joint attached to the elevation axis as shown in Fig. 1. Both joints are controller by DC Servo motors. The camera is mounted at the center of the inner joint. Besides these two axes that need to be controlled, the camera is mounted on a frame which can move freely in two degrees of freedom within a limited small angle. This frame and the camera are kept at the center position by magnetic field, so that shock vibration will be damped out effectively.

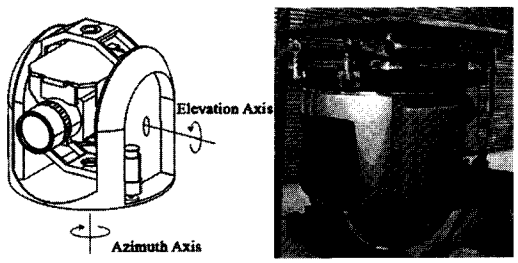

Figure 1: The two-axis gimbal configuration

3. Gimbal Kinematics

To obtain the kinematics equations of the gimbal, the well-known Denavit-Hartenberg convention will be used. There are three coordinate frames needed to be defined that consist of the gimbal base frame (B), the gimbal outer frame (O), and the gimbal inner frame (I).

3.1 Gimbal Components and Structure

The gimbal consists of two revolute joints where each joint is powered by DC Servo motors. The camera is not mounted directly to the inner joint but it is mounted to a frame attached to the center of the two axes as shown in Fig. 1 and Fig. 2. The frame can move freely in two degrees of freedom within a limited small angle. The magnetic field will be used to maintain the position of this frame to a pre-defined fixed position. This will stabilize the motion of the camera due to the undesired shock vibration.

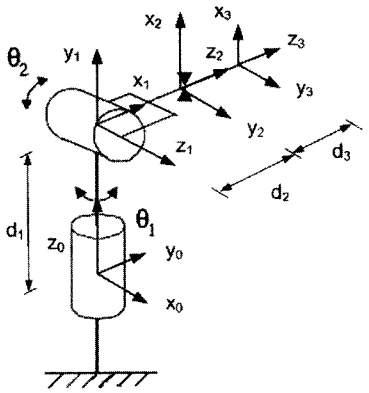

Figure 2: Link Frame Assignment

3.2 Forward Kinematics

The forward kinematics can be derived by using Denavit-Hartenberg convention as shown in Table 1.

Joint/Link i	α_i (rad)	a_i (m)	θ_i (rad)	d_i (m)	R/P
1	$-\pi/2$	0	θ_1	0	R
2	$\pi/2$	0	θ_2	0	R

Table 1: Denavit-Hartenberg parameter table.

The Homogeneous transformation from base (outer link) to the frame where the camera is attached (inner link) can be written as

$$T_0^2 = \begin{bmatrix} \cos\theta_1\cos\theta_2 & -\sin\theta_1 & \cos\theta_1\sin\theta_2 & 0 \\ \sin\theta_1\cos\theta_2 & \cos\theta_1 & \sin\theta_1\sin\theta_2 & 0 \\ -\sin\theta_2 & 0 & \cos\theta_2 & 0 \\ 0 & 0 & 0 & 1 \end{bmatrix} \quad (1)$$

where θ_1, θ_2 are the angle of the outer link and inner link, respectively.

3.3 Inverse Kinematics

The inverse kinematics problem is to find the joint variables given the end-effector position and orientation. Because the center or the origin of the two axes is located at the same point (at the center of mass of the gimbal), we can apply spherical a coordinate system at the

center of mass as shown in Fig. 3.

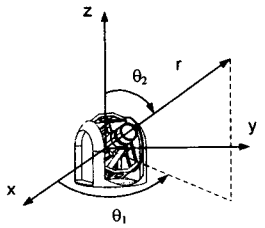

Figure 3: Spherical coordinate system

The coordinates based on the fixed frame of the gimbal can be easily written as $x = r\cos\theta_1 \sin\theta_2$, $y = r\sin\theta_1 \sin\theta_2$, $z = r\cos\theta_2$. And the inverse kinematics can be solved as $\theta_1 = \tan^{-1}\left(\frac{y}{x}\right)$, $\theta_2 = \tan^{-1}\left(\frac{\sqrt{x^2+y^2}}{z}\right)$, $r = \sqrt{x^2+y^2}$ where θ_1, θ_2 is the gimbal azimuth angle and elevation angle, respectively.

3.4 Differential Kinematics

Differential kinematics is used to find the relationship between the joint velocities and the end effector linear and angular velocity based on the gimbal fixed reference frame.

Geometric Jacobian

For an n-link manipulator, the geometric Jacobian is given by $\mathbf{J} = [\mathbf{J}_1 \ \cdots \ \mathbf{J}_n]$, where (both joint 1 and joint 2 are revolute joint):

$$\mathbf{J}_i = \begin{bmatrix} z_{i-1} \times (p - p_{i-1}) \\ z_{i-1} \end{bmatrix} \qquad (2)$$

where p describes the end-effector position. We can derive the Jacobian based on the Denavit-Hartenberg parameters. The Jacobian for both joints can be written as:

$$\mathbf{J}_{\omega_1} = \begin{bmatrix} 0 & 0 & 0 & 0 \\ 0 & 0 & 0 & 0 \\ 1 & 0 & 0 & 0 \end{bmatrix},$$

$$\mathbf{J}_{\omega_2} = \begin{bmatrix} 0 & -\sin\theta_1 & 0 & 0 \\ 0 & \cos\theta_1 & 0 & 0 \\ 1 & 0 & 0 & 0 \end{bmatrix}$$

4. Gimbal Dynamic Model

We can obtain the dynamic model of the gimbal using the Lagrange equation as follows:

4.1 Kinetic Energy

Consider a manipulator with n rigid links. The total kinetic energy is the sum of the contributions relative to the motion of each link and the contributions relative to the motion of each joint actuator. So, we can express the kinetic energy for an n-link robot manipulator in terms of Jacobian matrix and generalized coordinates as:

$$K = \frac{1}{2}\dot{q}^T \sum_{i=1}^{n} \left[m_i \mathbf{J}_{v_i}(q)^T \mathbf{J}_{v_i}(q) + \mathbf{J}_{\omega_i}(q)^T \mathbf{R}_i(q) \mathbf{I}_i \mathbf{R}_i(q)^T \mathbf{J}_{\omega_i}(q) \right] \dot{q}$$

where

$q = \begin{bmatrix} q_1 & \cdots & q_n \end{bmatrix}^T$ is the vector of joint variables. $\begin{bmatrix} v \\ \omega \end{bmatrix} = \begin{bmatrix} J_v \\ J_\omega \end{bmatrix} \dot{q}$

- v is end-effector linear velocity
- ω is angular velocity
- J_v is the $(3 \times n)$ matrix relative to the contribution of the joint velocity to the end-effector linear velocity.
- J_ω is the $(3 \times n)$ matrix relative to the contribution of the joint velocities to the end-effector angular velocity.
- $\mathbf{I}_i$ is the body moment of inertia about the rotation axis
- m_i is the link mass

So, the form of kinetic energy can be written as:

$$K = \frac{1}{2}\dot{q}^T \mathbf{D}(q) \dot{q} \qquad (3)$$

where $\mathbf{D}(q)$ is the inertia matrix and is a symmetric positive definite matrix.

4.2 Potential Energy

Potential energy for a robot manipulator is given by:

$$V = \sum_{i=1}^{n} V_i$$

where V_i is the potential energy of link i. If all links are rigid then potential energy is only caused by gravity as:

$$V_i = \int_{B_i} \mathbf{g}^T r_i dm = \mathbf{g}^T \int_{B_i} r_i dm = \mathbf{g}^T r_{ci} m_i \qquad (4)$$

where r_i is the position vector of the elementary particle, r_{ci} is the position vector of the link center of mass, $\mathbf{g} = \begin{bmatrix} 0 & 0 & g \end{bmatrix}^T$ is the gravity acceleration vector.

4.3 Lagrange Equation

The Lagrangian for an n-link robot manipulator can be written in terms of the kinetic energy and the potential energy as:

$$L = K - V = \frac{1}{2}\sum_{i=1}^{n}\sum_{j=1}^{n} d_{ij}(q)\dot{q}_i\dot{q}_j - V(q)$$

And the Lagrange equation is:

$$\frac{d}{dt}\frac{\partial L}{\partial \dot{\lambda}_i} - \frac{\partial L}{\partial \lambda_i} = F_i \qquad i = 1, 2, \ldots, n$$

where F_i is the generalized force associated with the generalized coordinate λ_i. And

$$\begin{bmatrix} \lambda_1 & \cdots & \lambda_n \end{bmatrix}^T = \begin{bmatrix} q_1 & \cdots & q_n \end{bmatrix}^T$$

So that, the dynamic equation can be expressed :

$$\sum_j d_{ij}(q)\ddot{q}_j + \sum_{j=1}^{n}\sum_{k=1}^{n} c_{ijk}(q)\dot{q}_k\dot{q}_j + g_i(q) = \tau_i$$

where c_{ijk} is Christoffel symbols and is defined :

$$c_{ijk} = \frac{\partial d_{ij}}{\partial q_k} - \frac{1}{2}\frac{\partial d_{jk}}{\partial q_i}$$

The friction force, F_s, will be added to the dynamic equations, so the equation of motion in matrix form can be written as:

$$\mathbf{D}(q)\ddot{q} + \mathbf{C}(q,\dot{q})\dot{q} + F_s \operatorname{sgn}(\dot{q}) + \mathbf{g}(q) = \tau \qquad (5)$$

where the elements of the matrix C is defined as:

$$c_{ij} = \sum_{k=1}^{n} c_{ijk}(q)\dot{q}_k$$

where $\mathbf{F_s}$ is an approximated friction force and function $\operatorname{sgn}(\dot{q}) = +1$ when $\dot{q}$ is positive and $\operatorname{sgn}(\dot{q}) = -1$ when $\dot{q}$ is negative.

For our system, n is equal to 2. So, each matrix in the dynamic equations can be written as:

$$\mathbf{D}(q) = \begin{bmatrix} \mathbf{I}_{1_{22}} + \mathbf{I}_{2_{11}}\sin^2\theta_2 + \mathbf{I}_{2_{33}}\cos^2\theta_2 & 0 \\ 0 & \mathbf{I}_{2_{22}} \end{bmatrix}$$

$$\mathbf{C}(q,\dot{q}) = \begin{bmatrix} \frac{1}{2}\omega_2(\mathbf{I}_{2_{11}} - \mathbf{I}_{2_{33}})\times\sin(2\theta_2) & \frac{1}{2}\omega_1(\mathbf{I}_{2_{11}} - \mathbf{I}_{2_{33}})\times\sin(2\theta_2) \\ -\frac{1}{2}\omega_1(\mathbf{I}_{2_{11}} - \mathbf{I}_{2_{33}})\times\sin(2\theta_2) & 0 \end{bmatrix}$$

where

$\mathbf{I}_{i_{jk}}$ is a member of row j and column k of moment of inertia of link i

$$\mathbf{I}_1 = \begin{bmatrix} 0.065 & 0 & 0 \\ 0 & 0.069 & 0 \\ 0 & 0 & 0.07 \end{bmatrix},$$

$$\mathbf{I}_2 = \begin{bmatrix} 0.018 & 0 & 0 \\ 0 & 0.024 & 0 \\ 0 & 0 & 0.025 \end{bmatrix}$$

$\mathbf{I}_1$ and $\mathbf{I}_2$ can be obtained by computer aided design software.

5. The Controller Design

The gimbal is composed of two rotating axes: an elevation axis and an azimuth axis in order to control the line of sight of the gimbal. Several techniques can be employed for controlling the gimbal motion as well as the way it is implemented. A PID controller is one of the most popular candidates among controllers used for motion control of each motor as shown in Fig. 4. For our system, due to disturbances from many sources that affect the motion of the controlled system, we need more advanced controllers which can stabilize the servo loop more effectively. The robust inverse dynamics control and the adaptive control are two candidates for inner loop control or motion control of our system. The indirect stabilization control configuration as shown in Fig. 5 is used to control the overall system, so that the gimbal camera can track the target or maintain its line of sight (LOS). It is called indirect because a stabilizer or rate sensor is mounted on the base of the system to measure the disturbance. The stabilizer can withstand high angular rates generated during slew and is equipped with a processor to transform the measurement to an equivalent disturbance about the LOS. The motors with controllers are inside the motor block in Fig. 5. The outer-loop controller, with angular rates and orientation information, is for cancellation of the disturbance due to motion of the airplane. A rate sensor is mounted on the base of the gimbal to measure base rate relative to the fixed earth reference frame. The base rate

will be transformed to LOS coordinates. The controller will compute commands to reject this disturbance.

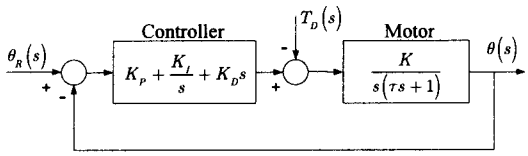

Figure 4: PID controller

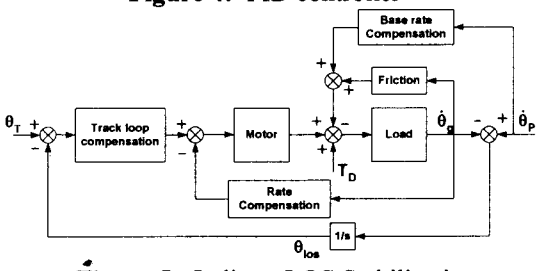

Figure 5: Indirect LOS Stabilization schematics

We are interested in the problem of tracking a joint space trajectory. The system is a nonlinear multivariable system as shown in equation (5). The controller technique called nonlinear state feedback can be used to obtain the global linearization of the system dynamics. This is the inverse dynamics control. From the dynamic equation (5), the control τ can be a function of the system state in the form:

$$\tau = \mathbf{D}(q)y + \mathbf{C}(q,\dot{q})\dot{q} + F_s \operatorname{sgn}(\dot{q}) + \mathbf{g}(q) \quad (6)$$

By applying this control, the system equation (5) can be described by:

$$\ddot{q} = y \quad (7)$$

where y can be considered as a new input vector whose expression is to be determined yet. And y can be selected as:

$$y = \ddot{q}_d + K_p(q_d - q) + K_D(\dot{q}_d - \dot{q}) + K_I\int_0^t (q_d - q)dt \quad (8)$$

where $q_d, \dot{q}_d, \ddot{q}_d$ are the desired joint trajectory, joint velocity, and joint acceleration. So, equation (7) can be turned into the homogeneous differential equation as:

$$\dddot{\tilde{q}} + K_D\ddot{\tilde{q}} + K_P\dot{\tilde{q}} + K_I\int_o^t \tilde{q}dt = 0 \quad (9)$$

where $\tilde{q} = q_d - q$. Equation (9) expresses the dynamics of position error, $\tilde{q}$, while tracking the given trajectory, $q_d, \dot{q}_d, \ddot{q}_d$. The gain K_P, K_D, K_I can be selected by specifying the desired speed of response. From equation (6), the control can be computed in real-time based on the parameters of the system dynamic model. In practice, it is difficult to obtain an accurate dynamic model especially in our case. Not only is the model inaccurate, but also the disturbances due to friction and environment change. The robust inverse dynamic and the adaptive control will be used instead.

5.1 Robust Inverse Dynamics Control

The control vector will be expressed by:

$$\tau = \hat{\mathbf{D}}(q)y + \hat{\mathbf{N}}(q,\dot{q}) \quad (10)$$

where

$\hat{\mathbf{N}}(q,\dot{q})$ is the estimate of:

$(\mathbf{C}(q,\dot{q})\dot{q} + F_s \operatorname{sgn}(\dot{q}) + \mathbf{g}(q))$

$\hat{\mathbf{D}}(q)$ is the estimate of $\mathbf{D}(q)$

The control design is based on the assumption that the error of the estimates or the uncertainty is bounded or can be estimated on its range of variation. Even though the uncertainty is unknown, the following assumption is necessary for the control design:

1) Maximum of $\ddot{q}_d$ exists or

$$\sup_{t\geq 0}\|\ddot{q}_d\| \leq Q_m < \infty \quad \textit{for all } \ddot{q}_d \quad (11)$$

2) Bound on Mass Matrix

$$\left\|\mathbf{I} - \mathbf{D}^{-1}(q)\hat{\mathbf{D}}(q)\right\| \leq a \leq 1 \quad \textit{for all } q \quad (12)$$

where $\mathbf{D}(q)$ is positive definite matrix with has upper and lower limited norms. So,

$$d_{\min} \leq \left\|\mathbf{D}^{-1}(q)\right\| \leq d_{\max} \quad (13)$$

$$\hat{\mathbf{D}} = \frac{2}{d_{\min} + d_{\max}}\mathbf{I} \quad (14)$$

$$\frac{2d_m}{d_{\min} + d_{\max}} \leq \left\|\mathbf{D}^{-1}(q)\hat{\mathbf{D}}(q)\right\| \leq \frac{2d_{\max}}{d_{\min} + d_{\max}} \quad (15)$$

From equation (12), (13), and (14), it is true that:

$$\left\|\mathbf{D}^{-1}(q)\hat{\mathbf{D}}(q)-\mathbf{I}\right\| \le \frac{d_{\max}-d_{\min}}{d_{\max}+d_{\min}} = a \le 1 \quad (16)$$

3) Bound on Non-linear terms

$$\left\|\hat{\mathbf{N}}(q,\dot{q})-\mathbf{N}(q,\dot{q})\right\| < \infty \quad \textit{for all } q,\dot{q} \quad (17)$$

Substitute equation (10) into equation (5), we obtain:

$$\mathbf{D}(q)\ddot{q}+\mathbf{N}(q,\dot{q}) = \hat{\mathbf{D}}(q)y+\hat{\mathbf{N}}(q,\dot{q}) \quad (18)$$

Rearrange equation (18), we will get:

$$\ddot{q} = y+\left(\mathbf{D}^{-1}(q)\hat{\mathbf{D}}(q)-\mathbf{I}\right)y + \mathbf{D}^{-1}\left(\hat{\mathbf{N}}(q,\dot{q})-\mathbf{N}(q,\dot{q})\right)$$

or

$$\ddot{q} = y-\Gamma \quad (19)$$

where

$$\Gamma = \left(\mathbf{I}-\mathbf{D}^{-1}(q)\hat{\mathbf{D}}(q)\right)y - \mathbf{D}^{-1}\left(\hat{\mathbf{N}}(q,\dot{q})-\mathbf{N}(q,\dot{q})\right) \quad (20)$$

From equation (8), let us select the input y is:

$$y = \ddot{q}_d+K_D\left(\dot{q}_d-\dot{q}\right)+K_P\left(q_d-q\right) + K_I\int_0^t\left(q_d-q\right)dt \quad (21)$$

So, equation (19) leads to:

$$\dddot{\tilde{q}}+K_D\ddot{\tilde{q}}+K_P\dot{\tilde{q}}+K_I\tilde{q} = \mathbf{N}(q,\dot{q}) \quad (22)$$

Equation (22) is still non-linear and coupled. It is not guaranteed that the error will converge to zero. Equation (19) can be rewritten as:

$$\ddot{q}_d-\ddot{q} = \ddot{q}_d-y+\Gamma \rightarrow \dddot{\tilde{q}} = \ddot{q}_d-y+\Gamma \quad (23)$$

Let define state variables as $\eta = \begin{bmatrix}\tilde{q}\\ \dot{\tilde{q}}\\ \ddot{\tilde{q}}\end{bmatrix}$

The state equation of equation (19) can be written as:

$$\begin{bmatrix}\dot{\eta}\\ \ddot{\eta}\end{bmatrix} = \begin{bmatrix}0 & \mathbf{I}\\ 0 & 0\end{bmatrix}\begin{bmatrix}\eta\\ \dot{\eta}\end{bmatrix}+\begin{bmatrix}0\\ \mathbf{I}\end{bmatrix}\left(\ddot{q}_d-y+\Gamma\right) \quad (24)$$

The input y can be selected as usual:

$$y = \ddot{q}_d+K_D\ddot{\tilde{q}}+K_P\dot{\tilde{q}}+K_I\int_0^t\tilde{q}dt+w \quad (25)$$

The term w is to be designed to guarantee robustness to the effects of uncertainty.

Substitute equation (25) into equation (24), we get:

$$\begin{bmatrix}\dot{\eta}\\ \ddot{\eta}\end{bmatrix} = \begin{bmatrix}0 & \mathbf{I}\\ 0 & 0\end{bmatrix}\begin{bmatrix}\eta\\ \dot{\eta}\end{bmatrix} + \begin{bmatrix}0\\ \mathbf{I}\end{bmatrix}\left(-K_D\ddot{\tilde{q}}-K_P\dot{\tilde{q}}-K_I\int_0^t\tilde{q}dt-w+\Gamma\right)$$

$$\begin{bmatrix}\dot{\eta}\\ \ddot{\eta}\\ \dot{\beta}\end{bmatrix} = \begin{bmatrix}0 & \mathbf{I} & 0\\ -K_P & -K_D & -K_I\\ \mathbf{I} & 0 & 0\end{bmatrix}\begin{bmatrix}\eta\\ \dot{\eta}\\ \beta\end{bmatrix}+\begin{bmatrix}0\\ \mathbf{I}\\ 0\end{bmatrix}(\Gamma-w) \quad (26)$$

where $\beta = \int_0^t\tilde{q}dt$. Equation (26) can be rewritten as:

$$\dot{\zeta} = \mathbf{H}\zeta+\mathbf{G}(\Gamma-w) \quad (27)$$

where $\zeta = \begin{bmatrix}\eta\\ \dot{\eta}\\ \beta\end{bmatrix}$,

$$\mathbf{H} = \begin{bmatrix}0 & \mathbf{I} & 0\\ -K_P & -K_D & -K_I\\ \mathbf{I} & 0 & 0\end{bmatrix},\quad \mathbf{G} = \begin{bmatrix}0\\ \mathbf{I}\\ 0\end{bmatrix}$$

For our system, ζ is a 6×1 vector. The gain K_P, K_D, K_I will be selected so that $\mathbf{H}$ will have eigenvalues with all negative real parts.

Using the Lyapunov direct method to derive the control function w is as follows:

Lyapunov function candidate

$$V = \zeta^T\mathbf{Q}\zeta > 0 \qquad \forall\zeta \quad (28)$$

where $\mathbf{Q}$ is a symmetric positive definite matrix

$$\dot{V} = \dot{\zeta}^T\mathbf{Q}\zeta+\zeta^T\mathbf{Q}\dot{\zeta} \quad (29)$$

$$\dot{V} = \zeta^T\left(\mathbf{H}^T\mathbf{Q}+\mathbf{Q}\mathbf{H}\right)\zeta+2\zeta^T\mathbf{Q}\mathbf{G}(\Gamma-w) \quad (30)$$

Because $\mathbf{H}$ has negative eigenvalues, so we will have:

$$\left(\mathbf{H}^T\mathbf{Q}+\mathbf{Q}\mathbf{H}\right) = -\mathbf{P} \quad (31)$$

where $\mathbf{P}$ is a symmetric positive definite matrix. So, equation (30) becomes:

$$\dot{V} = -\zeta^T\mathbf{P}\zeta+2\zeta^T\mathbf{Q}\mathbf{G}(\Gamma-w) \quad (32)$$

To make $\dot{V}$ negative definite, we will need $\|w\| \geq \|\Gamma\|$. So, it will be true that:

$$w = \frac{\rho}{\left\|\mathbf{G}^T\mathbf{Q}\zeta\right\|}\left(\mathbf{G}^T\mathbf{Q}\zeta\right), \quad \rho \geq \|\Gamma\| \qquad (33a)$$

For small value of $\left\|\mathbf{G}^T\mathbf{Q}\zeta\right\| < \varepsilon$, equation (33) will be modified to:

$$w = \frac{\rho}{\varepsilon}\left(\mathbf{G}^T\mathbf{Q}\zeta\right), \quad \left\|\mathbf{G}^T\mathbf{Q}\zeta\right\| < \varepsilon \qquad (33b)$$

The equation (33b) is to prevent chattering.

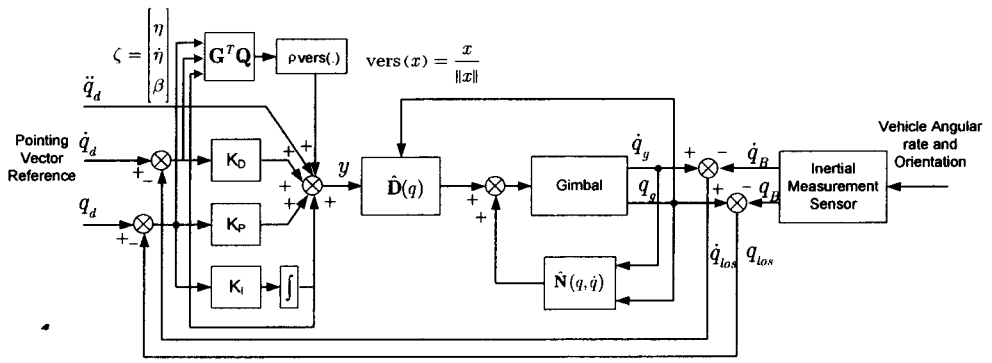

Figure 6: The block diagram of the robust inverse dynamics control

Fig. 6 shows the block diagram of the robust inverse dynamics control. An inertial measurement sensor is added to detect vehicle angular rate and orientation for outer loop control.

5.2 Adaptive Control

The robust inverse dynamics control described previously provide a rejection to external disturbances. It is also sensitive to the unmodeled dynamics and the rejection will be done at a high-frequency command action to keep the error trajectory on the sliding subspace. This may cause chattering and give an unacceptable control action. Adaptive Control is another control method for avoiding the possibility of chattering.

From equation (6), the dynamics model of the system is nonlinear in nature. We can rearrange the equation in linear form based on parameters of the model to:

$$\begin{aligned}\tau &= \mathbf{D}(q)\ddot{q} + \mathbf{C}(q,\dot{q})\dot{q} + F_s\,\text{sgn}(\dot{q}) + \mathbf{g}(q)\\ &= \mathbf{Y}(q,\dot{q},\ddot{q})\pi\end{aligned} \qquad (34)$$

where π is a $(p\times 1)$ vector of constant parameters and $Y(q,\dot{q},\ddot{q})$ is an $(n\times p)$ matrix which is a function of joint variables. As suggested by Slotine [12], the control law is:

$$\begin{aligned}\tau = \mathbf{D}(q)\ddot{q}_r + \mathbf{C}(q,\dot{q})\dot{q}_r + F_{s_r}\,\text{sgn}(\dot{q})\\ + \mathbf{g}(q) + K_D\sigma\end{aligned} \qquad (35)$$

where

$\dot{q}_r = \dot{q}_d + \Lambda\tilde{q}, \quad \ddot{q}_r = \ddot{q}_d + \Lambda\dot{\tilde{q}}$

K_D and Λ are positive definite matrices

$\sigma = \dot{q}_r - \dot{q}_d = \dot{\tilde{q}} + \Lambda\tilde{q}$

Using the Lyapunov direct method with the Lyapunov function as:

$$V(\sigma,\tilde{q}) = \frac{1}{2}\sigma^T\mathbf{D}(q)\sigma + \frac{1}{2}\tilde{q}^T\mathbf{M}\tilde{q} > 0 \quad \forall\sigma,\tilde{q} \neq 0 \qquad (36)$$

where $\mathbf{M} = 2\Lambda K_D$ is a symmetric positive definite matrix, and the fact that $\dot{\mathbf{D}} - 2\mathbf{C}$ is a skew-symmetric matrix, it can be proved that $\begin{bmatrix}\tilde{q}^T & \sigma^T\end{bmatrix}^T = 0$ is globally asymptotically stable for the control law as in equation (35).

Because the parameters of the model are not known exactly, the control law can be made adaptive to the vector parameters π. The control law equation (35), based on the estimated parameters of the model can be modified into:

$$\tau = \hat{\mathbf{D}}(q)\ddot{q}_r + \hat{\mathbf{C}}(q,\dot{q})\dot{q}_r + \hat{F}_{s_r}\,\mathrm{sgn}(\dot{q}) + \hat{\mathbf{g}}(q) + K_D\sigma \tag{37}$$

or

$$\tau = \mathbf{Y}(q,\dot{q},\ddot{q})\hat{\pi} + K_D\sigma \tag{38}$$

Substitution of equation (37) into equation (34) gives:

$$\begin{aligned}\mathbf{D}(q)\dot{\sigma} + \mathbf{C}(q,\dot{q})\sigma + F_{s_r}\,\mathrm{sgn}(\sigma) + K_D\sigma &= -\tilde{\mathbf{D}}(q)\ddot{q}_r - \tilde{\mathbf{C}}(q,\dot{q})\dot{q}_r - \tilde{F}_{s_r}\,\mathrm{sgn}(\dot{q}_r) - \tilde{\mathbf{g}}(q)\\ &= -\mathbf{Y}(q,\dot{q},\ddot{q})\tilde{\pi}\end{aligned} \tag{39}$$

where

$\tilde{\mathbf{D}} = \hat{\mathbf{D}} - \mathbf{D}$, $\tilde{\mathbf{C}} = \hat{\mathbf{C}} - \mathbf{C}$, $\tilde{F} = \hat{F} - F$, $\tilde{\mathbf{g}} = \hat{\mathbf{g}} - \mathbf{g}$, $F_{s_r} = F\dot{q}_r$ and $\tilde{\pi} = \hat{\pi} - \pi$

From the dynamic model equation (34) and the controller equation (37) or (38), we need to derive an adaptation to the vector parameter π by modifying the Lyapunov function as in equation (36) into the form:

$$V(\sigma,\tilde{q},\tilde{\pi}) = \frac{1}{2}\sigma^T D(q)\sigma + \tilde{q}^T\Lambda K_D\tilde{q} + \frac{1}{2}\tilde{\pi}^T K_m\tilde{\pi} > 0 \tag{40}$$

for all $\sigma,\tilde{q},\tilde{\pi} \neq 0$, K_m is a symmetric positive definite matrix.

Taking the time derivative of equation (40) along the trajectory of equation (39) gives:

$$\begin{aligned}\dot{V}(\sigma,\tilde{q},\tilde{\pi}) &= -\sigma^T F(q)\sigma - \dot{\tilde{q}}^T K_D\dot{\tilde{q}} - \tilde{q}^T\Lambda K_D\Lambda\tilde{q} + \tilde{\pi}^T\left(K_m\dot{\tilde{\pi}} - \mathbf{Y}^T(q,\dot{q},\dot{q}_r,\ddot{q}_r)\sigma\right)\\ \dot{V}(\sigma,\tilde{q},\tilde{\pi}) &= -\sigma^T F(q)\sigma - \dot{\tilde{q}}^T K_D\dot{\tilde{q}} - \tilde{q}^T\Lambda K_D\Lambda\tilde{q} + \tilde{\pi}^T\left(K_m\left(\dot{\hat{\pi}} - \dot{\pi}\right) - \mathbf{Y}^T(q,\dot{q},\dot{q}_r,\ddot{q}_r)\sigma\right)\end{aligned} \tag{41, 42}$$

So, the adaptive law for updating the parameter vector is:

$$\dot{\hat{\pi}} = K_m^{-1}\mathbf{Y}^T(q,\dot{q},\dot{q}_r,\ddot{q}_r)\sigma \tag{43}$$

Fig. 7 shows a block diagram of the adaptive control. The diagram also includes an inertial measurement sensor to detect vehicle angular rate and orientation for outer loop control

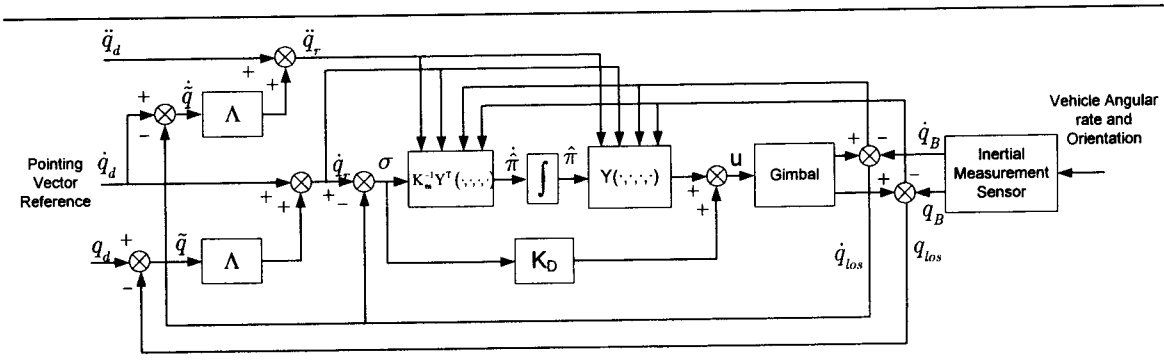

Figure 7: The block diagram of the adaptive control

6. Experimental Result

Fig. 8 shows the experimental setup. The gimbal is hung freely, so that a base rate disturbance can be generated to emulate close to the real situation. A rate sensor or inertial measurement sensor is mounted on the base of the gimbal to detect the base rate and base orientation reference to the fixed reference frame.

The objective of the control is to maintain LOS position while disturbances and base motion, disturb the system. Robust inverse dynamics control and the adaptive control are

implemented. To test the tracking capability, the reference trajectory $q_d, \dot{q}_d, \ddot{q}_d$ is generated from the trapezoidal velocity profile or s-profile trajectory. The gimbal is swung to generate the slew motion to create the environment motion close to the real situation.

Figure 8: Experimental and Environment Setup

A trapezoidal velocity profile is generated by setting traveling distance, maximum velocity, and maximum acceleration equal to 1 rad, 0.5 rad/sec, and 0.8 rad/sec^2 , respectively. The gains used in each controller are as follows:

Inverse dynamics control

$$K_P = \begin{bmatrix} 20 & 0 \\ 0 & 20 \end{bmatrix},\ K_D = \begin{bmatrix} 5 & 0 \\ 0 & 5 \end{bmatrix},\ K_I = \begin{bmatrix} 0.4 & 0 \\ 0 & 0.2 \end{bmatrix}$$

Robust inverse dynamics control

$$K_P = \begin{bmatrix} 20 & 0 \\ 0 & 20 \end{bmatrix},\ K_D = \begin{bmatrix} 5 & 0 \\ 0 & 5 \end{bmatrix},\ K_I = \begin{bmatrix} 0.4 & 0 \\ 0 & 0.2 \end{bmatrix}$$

$$Q = \begin{bmatrix} 3.8178 & 0 & 0.3409 & 0 & 6.3173 & 0 \\ 0 & 5.3707 & 0 & 0.6523 & 0 & 12.5461 \\ 0.3409 & 0 & 0.1682 & 0 & 1.25 & 0 \\ 0 & 0.6523 & 0 & 0.2305 & 0 & 2.5 \\ 6.3173 & 0 & 1.25 & 0 & 25.1363 & 0 \\ 0 & 12.5461 & 0 & 2.5 & 0 & 50.1305 \end{bmatrix}$$

$\rho = 10$, $\varepsilon = 0.04$, and $\mathbf{P} = diag(10)$

Adaptive control

$$\Lambda = \begin{bmatrix} 5 & 0 \\ 0 & 5 \end{bmatrix},\ K_D = \begin{bmatrix} 2.5 & 0 \\ 0 & 2.5 \end{bmatrix},\ K_m = \begin{bmatrix} 0.01 & 0 \\ 0 & 0.01 \end{bmatrix}$$

Fig. 9 and Fig 10 show the tracking performance of the trapezoidal velocity profile of the azimuth axis for various types of controller. The error shown in Fig. 10 and Fig. 12 are confirmed, that the robust inverse dynamics control and adaptive control perform better than the inverse dynamics control. And as mention previously, the robust inverse dynamics control provides a rejection to external disturbances. It is also sensitive to the unmodeled dynamics and the rejection will be done as a high-frequency command action to keep the error trajectory on the sliding subspace as noticed in Fig. 10 (b) and Fig. 12 (b). To prevent chattering during the low value of $\|\mathbf{G}^T\mathbf{Q}\zeta\| < \varepsilon$, equation (33b) is used instead. For the parameters, adaptation does not provide any action aimed to reduce the effects of external disturbances, but the action has a naturally smooth time behavior as illustrated in Fig. 10 (c) and Fig. 12 (c).

Indirect LOS Stabilization

A stabilizer or rate sensor is mounted on the base of the system to measure the disturbance due to the change in orientation of the aviation vehicle. The installed stabilizer can withstand high angular rates generated during slew and is equipped with a processor to transform the measurement to an equivalent disturbance about the LOS so that the camera can be locked to point to the target object. As shown in Fig. 6 and Fig. 7, the inertial measurement sensor can measure both orientations referenced to the fixed reference frame, and angular rate of the aviation vehicle. This measurement information is used for adjusting the reference command trajectory so that the camera will be maintained pointing to the target or LOS direction. To demonstrate the performance of indirect LOS stabilization of various controllers mentioned in this paper, the system disturbances is generated by the angular motion of the aerial vehicle. The disturbance is added in two cases. First, the disturbance is added while the gimbal is moving to the new target. Second, the disturbance is added when the gimbal is pointing to the target.

Fig. 13 and Fig. 14 show the response of the robust inverse dynamics control of the azimuth angle and the pitch angle, respectively, when the gimbal is shacked about 12 second and released while maintaining its LOS direction. The same situation is applied for the adaptive control as shown in Fig. 15 and Fig. 16 for azimuth angle

and pitch angle, respectively. Due to gravity, the disturbance in the pitch angle is rougher than the disturbance in the azimuth angle from the same shacking input. Near the reference LOS, the small disturbance in azimuth angle and pitch angle can be reduced by applying a magnetic field created from magnets installed at the gimbal shell and inner axis. The magnetic field also helps to reduce settling time. The system also has a vertical vibration absorbing mechanism installed at the base, where the gimbal is attached to the aviation vehicle, to absorb shock vibration in the vertical direction.

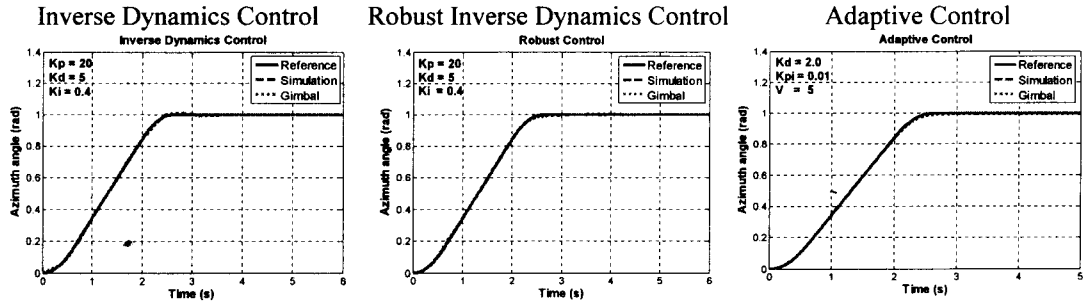

Figure 9: Tracking the trapezoidal velocity profile of azimuth axis (outer axis)

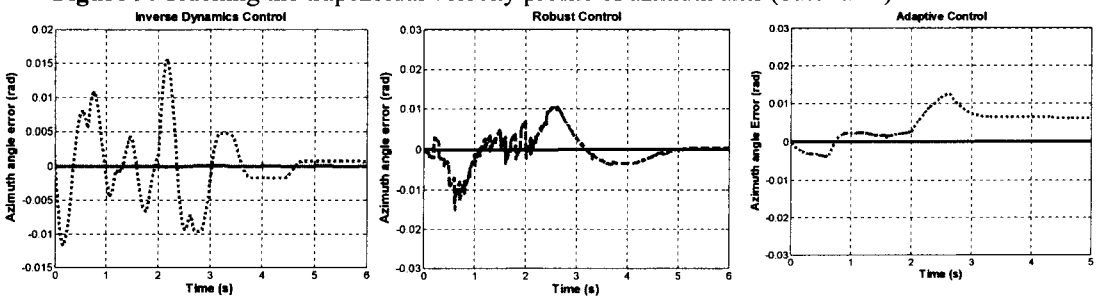

Figure 10: Error of the tracking of the azimuth axis

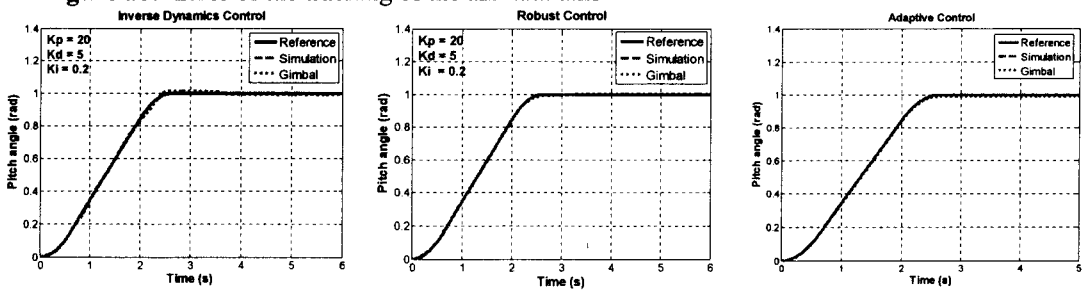

Figure 11: Tracking the trapezoidal velocity profile of elevation axis or pitch angle (inner axis)

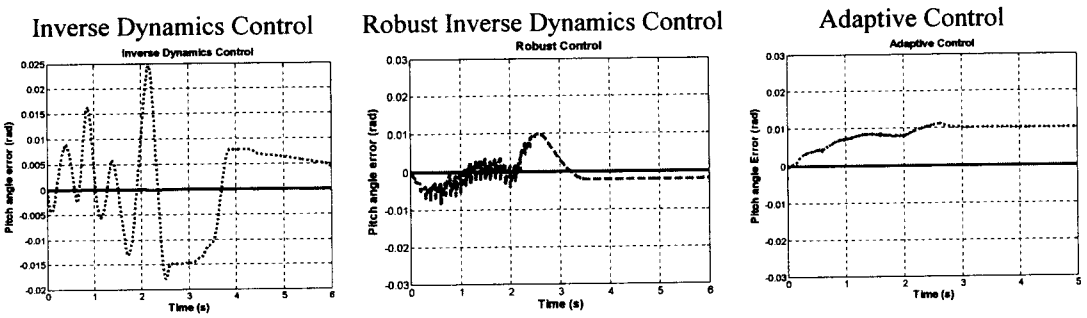

Figure 12: Error of the tracking of the elevation axis or pitch angle

Next, we change the LOS direction. This means that the control system has to follow the non-zero reference input in each axis of the gimbal. The controller must track the input and reject the base rate disturbance at the same time. The disturbance is in the form of shaking the base. The results are shown in Fig. 17 and Fig. 18 for azimuth and pitch angle, respectively. Similar results can be obtained from the adaptive control and will not be shown here. For the last experiment, we create a reference command close to the real situation. The reference command will be a sinusoidal function and the disturbance due to the orientation change of the aviation vehicle will be a random swing applied at the base. The response of the azimuth axis for the robust inverse dynamic and the adaptive control are shown in Fig. 19 and Fig. 20, respectively. The experimental results show that the robust inverse dynamics control and the adaptive control perform very effective for our inertial stabilization system, and are very promising controllers.

7. Conclusion

The details of the two controllers, the robust inverse dynamic and the adaptive control, of a two-axes gimbal (azimuth or base rotation and pitch or elevation) configuration are described. The experiments are done with various command references with disturbances due to error in dynamics model and consists of: friction force, gravity force and coriolis and centripetal force, the disturbance due to orientation of the aviation vehicle where the gimbal attached to, and the disturbance due to environment change (in the form of bounded disturbance). The robust inverse dynamic and the adaptive control can be used for low-level motion control of the gimbal. A stabilizer or rate sensor is mounted on the base of the system to measure the disturbance due to the change in orientation of the aviation vehicle. The installed stabilizer is equipped with a processor to transform the measurement to an equivalent disturbance about the LOS, so that the camera can be locked to point to the target object. Indirect stabilization is for reducing the jittering due to base rate disturbances. Unbalanced mass and friction can also be compensated by integral action.

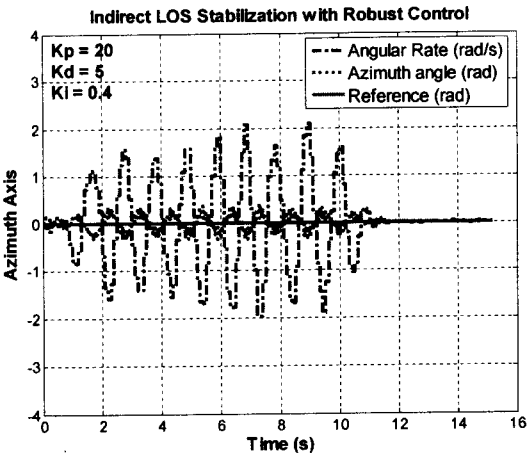

Figure 13: The response of the robust inverse dynamics control to vibrating of the azimuth angle.

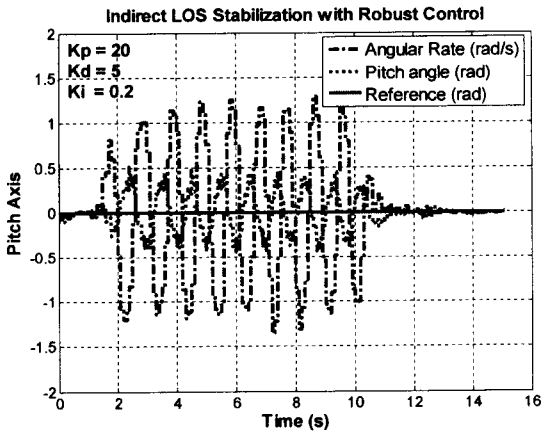

Figure 14: The response of the robust inverse dynamics control to vibrating of the pitch angle.

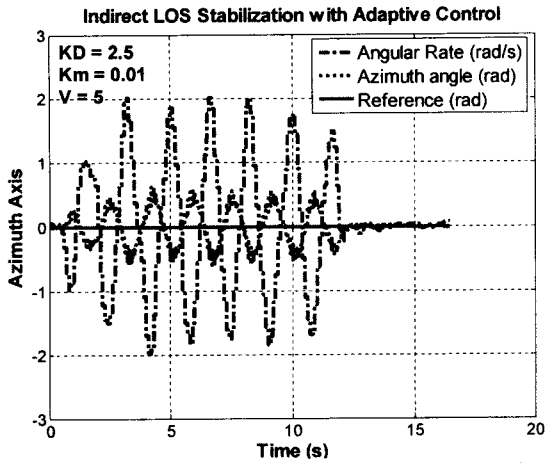

Figure 15: The response of the adaptive control to vibrating of the azimuth angle.

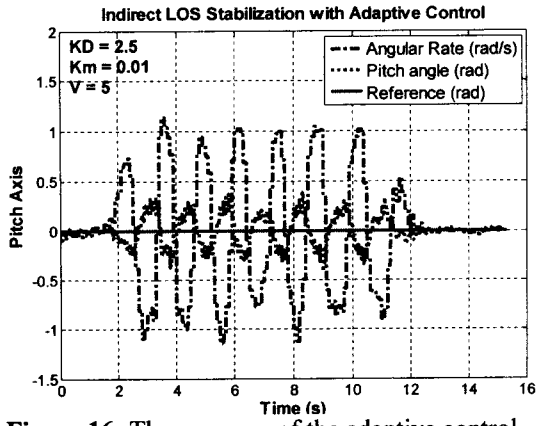

Figure 16: The response of the adaptive control to vibrating of the pitch angle.

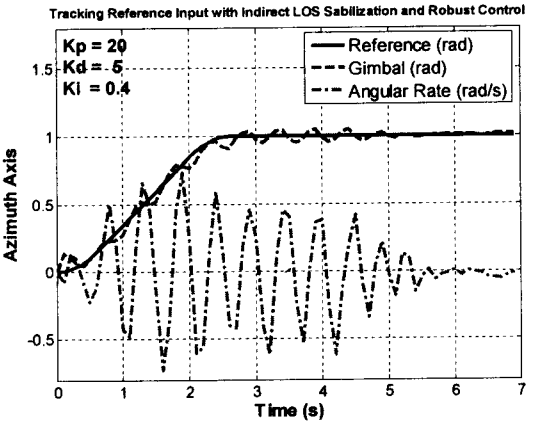

Figure 17: The response of azimuth axis, using the robust inverse dynamics control, while the disturbance is exited, during the gimbal move to the new target.

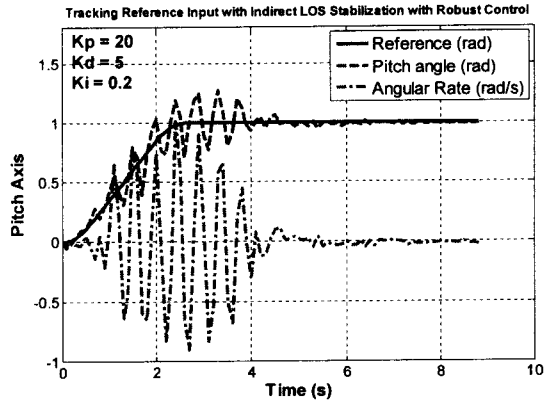

Figure 18: The response of pitch axis, using the robust inverse dynamics control, while the disturbance is exited, during the gimbal move to the new target.

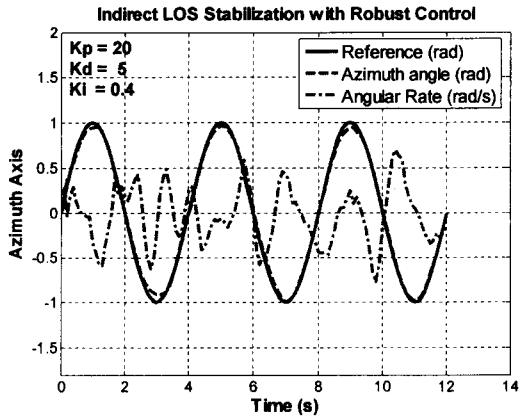

Figure 19: The response of azimuth axis, using robust inverse dynamics control, when the input is a sinusoidal function, generated by random swing disturbance applied to the base.

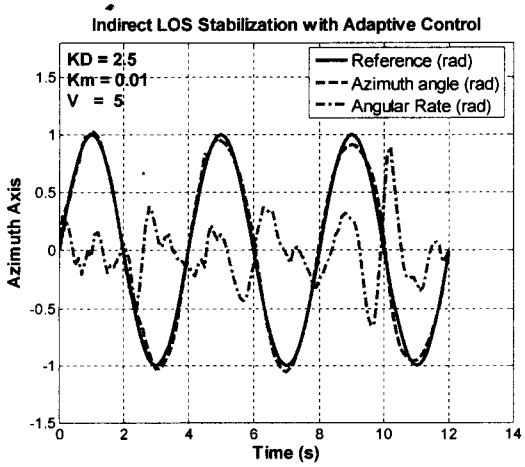

Figure 20: The response of azimuth axis, using adaptive control, when the input is a sinusoidal function, generated by random swing disturbance applied to the base.

8. References

[1] Peter J. Kenady, Direct Versus Indirect Line of Sight (LOS) Stabilization, IEEE Transactions on Control Systems Technology, Vol. 11, No.1, January 2003.

[2] Bo Li, David Hullender, Mike DiRenzo, Nonlinear Induced Disturbance Rejection in Inertial Stabilization Systems, IEEE Transactions on Control Systems Technology, Vol. 6, No.3, May 1998.

[3] Per Skoglar, Modelling and Control of IR/EO-gimbal for UAV Surveillance Applications, Master's thesis, Department of Electrical Engineering, Linköping University, Sweden.

[4] John J. Craig, Introduction to Robotics Mechanics and Control, Silma, Inc., 1989.

[5] H. Ambrose, Z. Qu, R. Johnson, Nonlinear Robust Control For A Passive Line-of-Sight Stabilization System, Proceedings of the 2001 IEEE International Conference on Control Applications, September 5-7, 2001.

[6] T.H. Lee, E.K. Koh, M.K. Loh., Stable Adaptive Control of Multivariable Servomechanisms, with Application to a Passive Line-of-sight Stabilization System, IEEE Transactions on Industrial Electronics, Volume: 43, Issue: 1, Pages: 98– 105, Feb 1996.

[7] Junhong Nie, Fuzzy Control of Multivariable Nonlinear Servomechanisms with Explicit Decoupling Scheme, IEEE Transactions on Fuzzy Systems, Volume: 5, Issue: 2, Pages: 304 – 311, May 1997.

[8] Bo Li, David Hullender, Self-Tuning Controller for Nonlinear Inertial Stabilization System, IEEE Transactions on Control Systems Technology, Vol. 6, No.3, May 1998.

[9] Gregory Becker, Ronald Cubalchini, Quang Tham, John Anagnost, Generation of Structural Design Constraints for Spaceborne Precision Pointing System, Proceedings of the 2001 IEEE International Conference on Control Applications, Hawaii, USA, August 1999.

[10] Sungpil Yoon, John B. Lundberg, Equations of Motion for a Two-Axes Gimbal System, IEEE Transactions on Aerospace and Electronic System, Vol. 37, No.3, July 2001.

[11] Clément M, Gosselin, Jean-François Hamel, The Agile Eye: a High-performance three-Degree-of-freedom Camera-orienting Device, 1994, Proceedings of the 1994 IEEE.

[12] Slotine, J.-J.E.: Robust Control of Robot Manipulators, Int. J. Robotics Research, Vol. 4, No. 2, 1987.